Modeling Macrosegregation with a Multiphase Approach: Examples and Discussions

Menghuai Wu and Andreas Ludwig

Simulation and Modeling of Metallurgical Processes,
Department of Metallurgy, University of Leoben, A-8700 Leoben, Austria
menghuai.wu@mu-leoben.at

A multiphase approach is used to study the macrosegregation phenomena that occur during solidification. Some modeling examples with accompanying animations are presented to increase the understanding of different mechanisms of macrosegregation formation. Examples are presented consecutively with increasing complexity of the mechanisms: (1) macrosegregation in columnar solidification; (2) macrosegregation in globular equiaxed solidification; (3) macrosegregation in the mixed equiaxed-columnar solidification; (4) Marangoni convection induced macrosegregation.

INTRODUCTION

Knowledge of macrosegregation phenomena in castings has increased significantly in the past few decades, including the development of different analytical and numerical models to study and predict such phenomena in different casting processes [1-3]. Macrosegregation occurs due to the relative motion between different phases during solidification. This relative motion between phases can arise as a result of thermosolutal convection, solidification shrinkage induced flow, flotation and sedimentation of free moving grains, forced flow by stirring mechanically or electromagnetically, flow caused by pore or gas bubble formation, deformation of the solid framework, capillary (Marangoni) force induced flow, etc [1-5]. As summarized by Beckermann: 'while some successes have been reported in predicting measured macrosegregation patterns in industrially relevant casting processes, there are still numerous areas where further development is required [2].' Obviously, this article can not cover the entire range of macrosegregation phenomena, thus the current focus is limited to the authors' recent contributions to this topic. As such, specific examples of macrosegregation in columnar solidification, in globular equiaxed solidification, in mixed equiaxed-columnar solidification, and Marangoni induced macrosegregation are presented and discussed. Details about the numerical models are presented elsewhere [6-10].

MACROSEGREGATION IN COLUMNAR SOLIDIFICATION

The benchmark (Figure 1) of a steel ingot with reduced size is simulated. A two-phase columnar solidification model is used. The purpose is to study the macrosegregation due to mechanism of thermosolutal convection during columnar solidification. Details about process and thermo physical parameters can be found in previous publications [5,8]. The important model assumptions are summarized as follows:

1. Mold filling is not simulated, solidification starts with an initial concentration Fe-0.34 wt.%C and an initial temperature 1785 K;
2. Two phases are considered: the melt and columnar dendrite trunks;
3. Columnar dendrite morphology is approximated by step-wise growing cylinders with constant primary arm spacing;
4. Boussinesq approximation is used to treat the thermosolutal convection;
5. Columnar trunks start from side and bottom walls;
6. Columnar tip front is tracked;
7. 2D axis symmetrical calculation is performed;
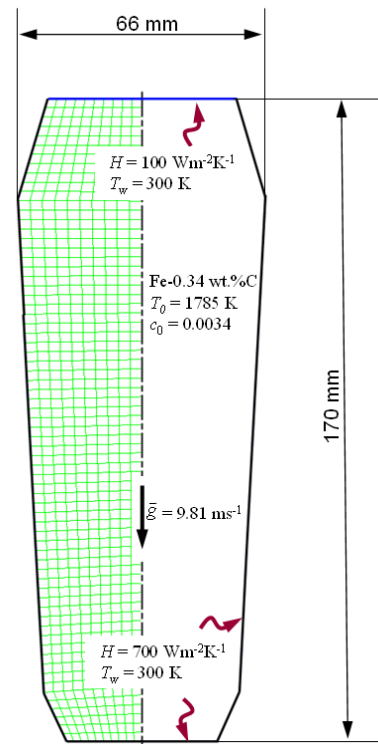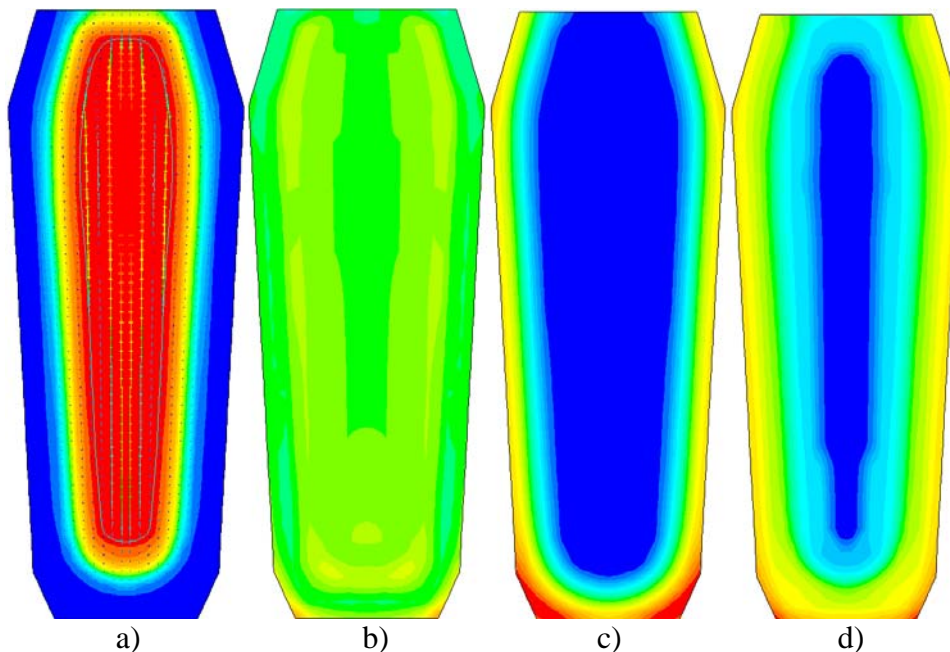8. Constant surface heat transfer coefficients are used (Figure 1).

Figure 1. Schematic of a reduced steel ingot.

a)   b)   c)   d)

Animation 1. Simulated solidification sequence and macrosegregation formation (Fe-0.34 wt% C),   a) volume fraction of columnar dendrite trunks f_c scaled from 0 (red) to 1 (blue), and the liquid velocity $\bar{u}_1$,   b) mix concentration c_{mix} scaled from 0.28 wt.% (blue) to 0.4 wt.% (red), c) liquid concentration c_l scaled from 0.34 wt.% (blue) to 4.3 wt.% (red), and d) solid concentration c_s scaled from 0.0984 wt.% (blue) to 0.38 wt.% (red).

The solidification process is shown in Animation 1. Columnar trunks start to grow from mold wall, the columnar tip front advances from the mold wall towards the bulk melt. Due to the influence of the thermosolutal convection, the 'hot spot' moves upwards and is finally located above the geometrical and thermal center of the casting. During solidification two axis-symmetric convection vortices develop. The melt near the mold wall has a higher density due to its lower temperature ($\beta_T = 2.x10^{-4}$ K^{-1}), and sinks downwards. The hotter melt in the center rises. One may argue that the solute-enriched interdendritic melt might partially compensate or reverse the above mentioned convection pattern. The liquid concentration c_l near the mold wall is much higher compared to the bulk melt region. With $\beta_c = 1.1x10^{-2}$ wt.%$^{-1}$, the higher the c_l, the lighter the interdendritic melt. Due to the high temperature gradient in the casting, however, the thermal buoyancy has a greater impact on the fluid motion than the solutal buoyancy. The downwards flow in the interdendritic regions and the upwards flow in the bulk melt is the basic phenomena which leads to the formation of the final macrosegregation pattern.

The positive macrosegregation in the center is formed gradually during solidification. The interdendritic melt always has a higher concentration than in the bulk melt. The interdendritic solute-enriched melt is brought out of the mushy zone by the flow current, causing the c_{mix} in front of, or slightly behind, the columnar tip front to be enriched gradually. These positively segregated areas of the melt are not stationary; they move with the flow current and finally meet in the casting center forming a large positive segregation zone.
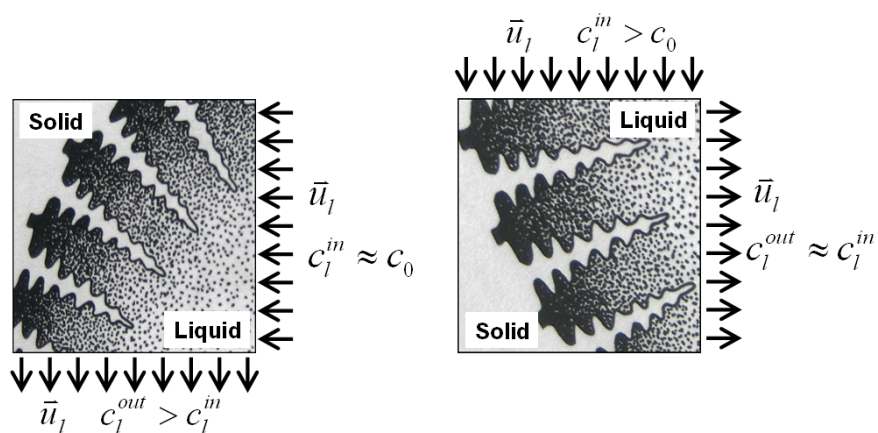
a) A sample volume in the upper corner.   b) A sample volume in the bottom corner.

Figure 2. Schematic illustration of negative and positive macrosegregation formation due to interdendritic flow (taken from literature[11] with modification).

Figure 2 illustrates the macrosegregation formation mechanism in the corner regions. A local volume taken from the upper corner of the ingot is considered in Figure 2a. The solidified columnar trunks are stationary, while the interdendritic melt flows, e.g. it flows in from a

horizontal side of the volume and out from a vertical. Due to solidification the interdendritic melt is segregated with solute elements ($k < 1$), c_1 is larger than the bulk melt concentration c_0. Melt with $c_1^{out} > c_0$ flows out of the volume, being replaced with 'fresh' melt with nearly the bulk concentration $c_1^{in} \approx c_0$. The consequence is that c_{mix} in the volume decreases, i.e. a negative macrosegregation occurs. In the lower bottom corners, Figure 2b, melt with $c_1^{in} > c_0$ flows vertically into the volume. This incoming melt is enriched in solute due to segregation in the solidifying interdendritic region along the mold wall. As the solidification now takes place from that segregated melt, the solid forms with a higher concentration $k \cdot c_1^{in}$ compared to $k \cdot c_0$, thus a positive macrosegregation forms.

MACROSEGREGATION IN GLOBULAR EQUIAXED SOLIDIFICATION

The benchmark (Figure 3) of an Al-4.0wt.%Cu die casting with a two-phase globular equiaxed solidification model is simulated. The purpose is to study the macrosegregation formed by mechanisms of grain sedimentation, and sedimentation induced convection during equiaxed solidification. Details about process and thermo physical parameters can be found in previous publications [6, 12]. The general model descriptions and assumptions are summarized:

1. Mold filling is not simulated, solidification starts with an initial concentration Al-4.0 wt.%Cu and an initial temperature 925 K;
2. Two phases are considered: the melt and equiaxed grains;
3. The grain morphology is approximated by spheres;
4. A three-parameter heterogeneous nucleation law is used;
5. Buoyancy force for the moving grains and thermosolutal convection are accounted for by a Boussinesq approximation.
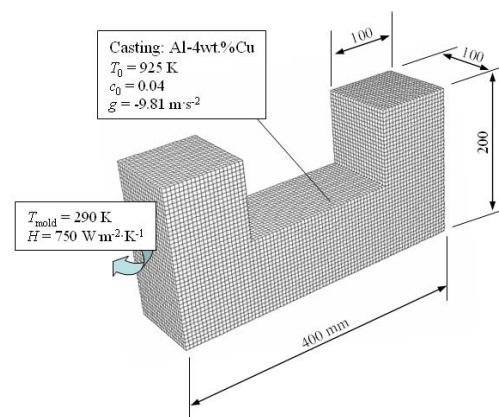

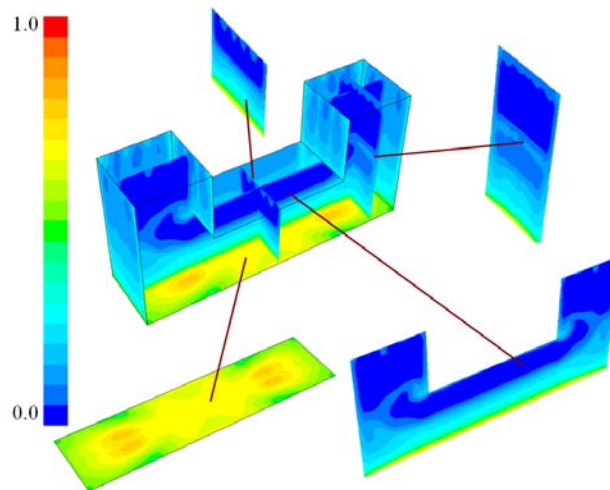Figure 3. Schematic of an aluminum alloy die casting.

Figure 4. Simulated phase distribution at 10 s after start of cooling. Volume fraction of the equiaxed phase f_s is shown in different sections with a color scale from 0 (blue) to 1 (red).

A 3D overview of the equiaxed phase distribution at 10 s after start of cooling is shown in Figure 4. The dynamic evolution sequences of the equiaxed phase, the sedimentation, and the induced macrosegregation are demonstrated in Animation 2. Grains which nucleate in the upper regions and at the sidewalls sink downwards. The sinking grains lead to an accumulation of the solid phase in the bottom region of the casting. The grains stop moving and finally settle, at the latest when the local fraction of solid exceeds the packing limit (0.637). The grain settlement is the main reason for the negative segregation at the bottom of the casting. As solidification proceeds, this negative segregation zone becomes wider and wider. The strongest negative segregations are found in the lower corners near the sidewalls, where the grains tend to accumulate and settle. As the residual positively segregated melt is separated from the sedimentation zone by the settling of grains, a positive segregation zone is formed nearby. It is generally observed that a positive segregation zone exists just near a sedimentation zone. This positively segregated zone is located within the melt, thus it is not stationary and may move with the melt flow. While solidification proceeds, the positively segregated melt areas move towards and accumulate gradually in the last-to-solidify region, forming a large positively segregated zone in the late stage of solidification.

| a) | b) |
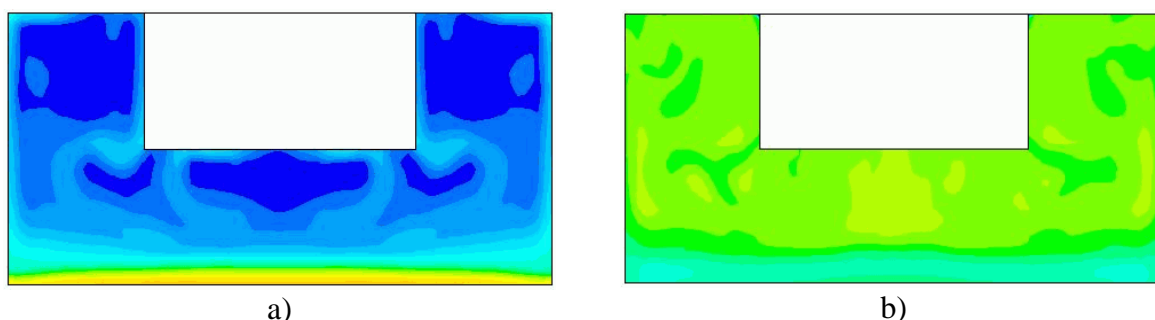
Animation 2. Simulated phase evolution, and the macrosegregation formation (Al-4.wt%Cu): a) volume fraction of columnar f_s scaled from 0 (red) to 1 (blue), b) mix concentration c_{mix} scaled from 3.15 wt.% (blue) to 4.85 wt.% (red).

MACROSEGREGATION IN MIXED EQUIAXED-COLUMNAR SOLIDIFICATION

The same benchmark as Figure 1 is simulated. 3D calculation is carried out. This benchmark shows a complex case of macrosegregation formation with the mechanisms of coupled thermosolutal convection, grain sedimentation, and sedimentation induced convection. Details about process and thermo physical parameters can be found in previous publications [8]. The important model assumptions are summarized:

1. Mold filling is not simulated, solidification starts with an initial concentration Fe-0.34 wt.%C and an initial temperature 1785 K;
2. Three phases are considered: the melt, equiaxed grains and columnar dendrite trunks;
3. Morphologies are approximated by step-wise growing cylinders for columnar dendrite trunks and spheres for equiaxed grains;
4. The buoyancy force of the moving grains and the thermosolutal convection are accounted for by a Boussinesq approximation;
5. A three-parameter heterogeneous nucleation law is used for the nucleation of the equiaxed grains, no fragmentation and grain attachment;
6. Columnar trunks start from side and bottom walls;
7. Columnar tip front is tracked;
8. Hunt's blocking mechanism [13] is applied for predicting CET.

The simulated solidification sequence including sedimentation of the equiaxed grains, sedimentation-induced melt convection and thermosolutal melt convection are shown in Figure 5 and Animation 3. The solidification pattern agrees with the classical explanation of steel ingot solidification, summarized by Campbell [14]. The columnar dendrites grow from the mold wall and the columnar tip front moves inwards. The equiaxed grains nucleate near the mold walls and in the bulk melt. The columnar dendrites are stationary, whereas the equiaxed grains sink and settle in the base region of the ingot. The accumulation of such grains at the base of the ingot has a characteristic cone-shape. Two symmetrical melt convection vortices in the ingot are induced by both thermosolutal effects and the drag of sinking grains. The sedimentation of grains and occurring melt convection influence the macroscopic solidification sequence and thus, the final phase distribution: more equiaxed grains will be found at the bottom and in the base region, and larger columnar areas in the upper part of the ingot.
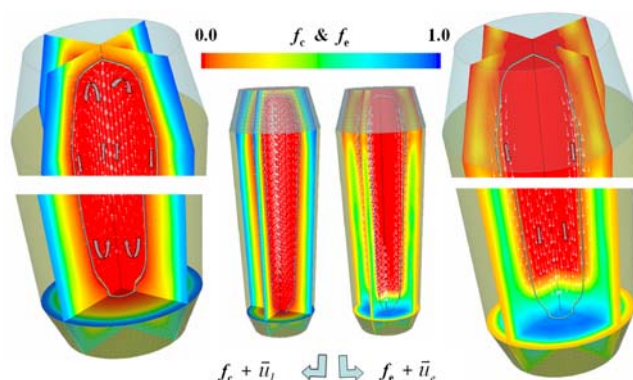
Figure 5. Simulated solidification sequence (at 20 s) of the steel ingot. f_c and f_e are shown in color scale in two vertical and one horizontal sections, while the velocity fields $\vec{u}_l$ and $\vec{u}_e$ are shown as vectors. The columnar tip front position is also shown.
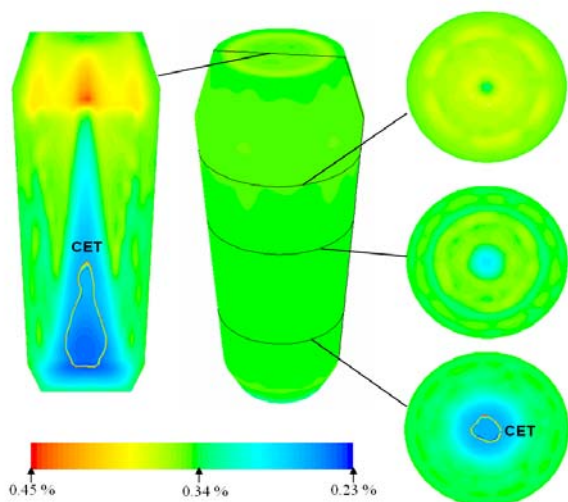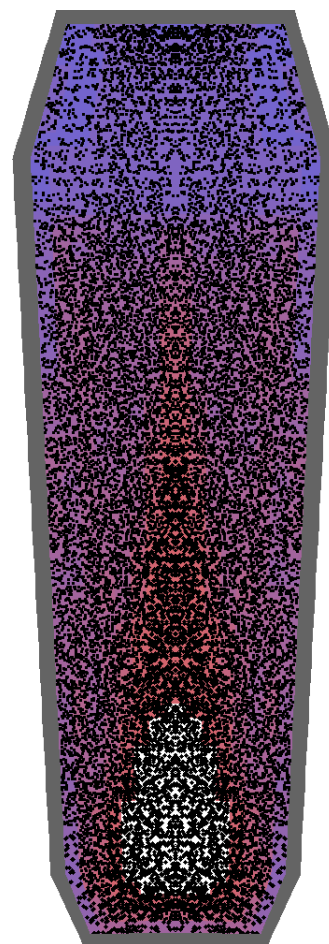

Figure 6. Predicted mix concentration c_{mix} in the steel ingot, scaled from 0.23 wt.% C (blue) to 0.45 wt.% C (red). The area of 100% equiaxed macrostructure is surrounded by CET line.

Animation 3. Dynamic of the mixed equiaxed-columnar solidification process. The equiaxed grains are shown with black dots. The number density and the size of the grains are reduced and enlarged to the scale that they can be seen with the naked eye. The progress of the columnar front and the evolution of the columnar phase are indicated with the color background.

As the columnar tip front is explicitly tracked in the model, the simulation shows that the columnar tip fronts from both sides tends to meet in the center of the casting. However, in the lower part of the casting the large amount of equiaxed grains stops the propagation of the columnar tip front. Its final position indicates the so-called columnar to equiaxed transition i.e. CET. The CET separates areas where only equiaxed grains appear from areas where both columnar dendrites and equiaxed grains might be found.

The final macrosegregation distribution is predicted, as shown in Figure 6. From the simulation results it becomes obvious that the main mechanism for the cone-shaped negative segregation in the base region is grain sedimentation. Since the settling grains are poor in solute elements, their pile-up results in negative segregation in the bottom of the ingot. A further contributing factor to the strength of negative segregation arises from the flow divergence of the residual liquid through this zone at a late solidification stage. The positive

segregation at the top region of the ingot is caused by the flow of the segregated melt in the bulk region. This kind of positive segregation coincides with classical experimental results as well [13]. It should be noted that channel segregations, which are frequently found in steel ingots, are not predicted in such a reduced ingot with the recent model.

MARANGONI CONVECTION INDUCED MACROSEGREGATION

The multiphase solidification approach discussed above is applied to model the spatial phase separation and macrosegregation caused by thermo-capillary force induced convection, i.e. Marangoni convection in a hypermonotectic alloy. As shown in Figure 7, when a hypermonotectic alloy with initial concentration c_0 is cooled down below the binodal, a secondary liquid phase (L_2) is decomposed in form of droplets from the parent melt (L_1). The surface tension between L_1 and L_2 is a function of the temperature. Therefore, due to the temperature gradient during solidification local convections inside and around the droplet is established. As consequence, this thermo-capillary force induced convection leads to the droplet moving from cold towards hot regions.

A 2D benchmark of Al-10.wt.%Bi alloy with a square cross section is simulated. During solidification of this alloy, as shown by the phase diagram (Figure 7), at least four phases appear: the parent melt L_1, the secondary liquid phase L_2, the solidified monotectic matrix and the solidified secondary phase. For simplicity our approach considers only two phases: L_1 and L_2. During monotectic reaction the monotectic matrix is transformed directly from L_1. Therefore the solidified monotectic matrix is modeled as phase L_1 in such a way that an enlarged viscosity is applied to phase L_1 upon reaching the monotectic temperature. The latent heat of the monotectic reaction is added to phase L_1. L_2 droplets appearing at the monotectic reaction front are modeled to be entrapped in the monotectic matrix by applying a similar enlarged viscosity at or below the monotectic point. Additional assumptions are as follows:

1. Filling is not simulated, solidification starts with an initial concentration Al-10 wt.%Bi and an initial temperature 1065 K;
2. Morphology of L_2 is approximated by spherical droplets;
3. A 3-parameter heterogeneous nucleation law for L_2 droplets is used, no collision and coalescence (coagulation) of the droplets is considered;
4. Growth of the droplets are controlled by diffusion in L_1;
5. Marangoni force and buoyancy force are treated by Boussinesq approximation;
6. Both liquid L_1 and L_2 phases have same viscosity;
7. Solidification of L_2 is ignored.

Two different simulations are made: one without gravity force, and with gravity force. The results of them are shown in Figure 8 and Animation 4.

For the case of 0-g, Marangoni motion presents the only mechanism for the phase transport. Droplets of L_2 start to nucleate and grow in the casting surface as the local temperature drops below the binodal (1062.2 K). The Marangoni force causes the L_2 droplets to move from surface region towards the casting center. The parent melt moves in reverse direction, because the space of the leaving phase L_2 must be replaced by the parent melt L_1. The movement of L_2 results in depletion of the L_2 phase (f_2) in the corners and surface regions, and enrichment of L_2 phase in the casting center. As cooling of the casting continues to the monotectic point, the monotectic reaction occurs, the velocity of L_1 vanishes, and the L_2 droplets are entrapped in the monotectic matrix. When solidification is finished, the surface has a lower volume fraction of L_2 phase than the sample center. The spatial separation of the phases is directly responsible for the macrosegregation: $c_{mix} < 7.2\%$Bi in corners, $c_{mix} > 12\%$Bi in center.

For the case with gravity, both buoyancy force and Marangoni force contribute to the movement of the L_2 droplets. The droplets nucleate in the corners and along the walls, then

grow and sink downwards along the vertical walls. The parent melt L_1 phase is drawn by the sinking L_2 droplets, forming two symmetric vortices: one clockwise in the right half and one anticlockwise in the left half of the casting. The convection currents of L_1 are so strong that they in turn influence the movement and the distribution of L_2 droplets. With the monotectic reaction the L_2 droplets are entrapped in the monotectic matrix; the phase and droplet size distribution remain unchanged afterwards. The final solidification results show the depletion of phase L_2 in the upper region and an enrichment of L_2 in the central bottom region. Strong spatial separation of the phases leads to a strong macrosegregation: $c_{\text{mix}} < 5\%$ Bi in the upper region, $c_{\text{mix}} > 25\%$ Bi in the lower bottom region. In this case, although both Marangoni motion and gravity induced droplet motion are considered in the case with g, no influence of Marangoni motion on the solidification result is seen. The function of the gravity overwhelms the Marangoni force under normal terrestrial conditions.
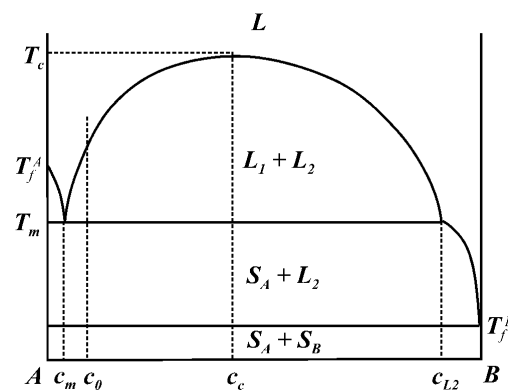

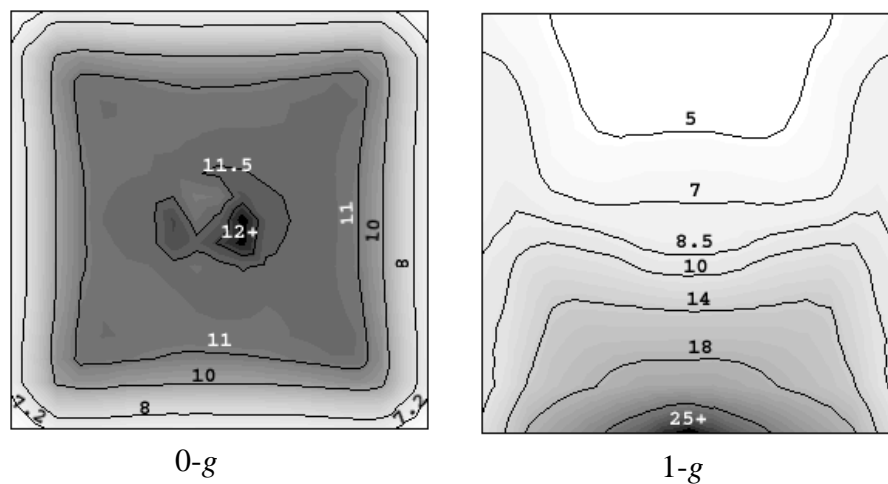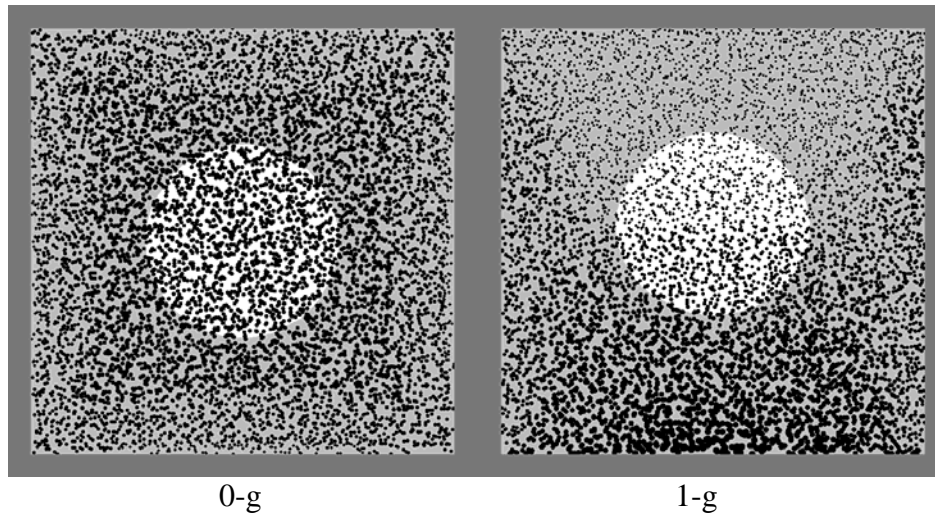Figure 7. Schematic phase diagram for a system with a liquid miscibility gap.

0-g

1-g

Figure 8. Numerically predicted Bi (wt.%) segregation in the solidified samples with initial concentration Al-10wt.%Bi. Left: no gravity, only Marangoni convection; Right: with gravity 1-g, and Marangoni convection.

0-g   1-g

Animation 4. Dynamic of the hypermonotectic solidification process. The droplets of L_2 are shown with black dots. The number density and the size of the droplets are reduced and enlarged to the scale that they can be seen with the naked eye. The progress of the monotectic reaction front and the evolution of the solidified matrix are indicated with the dark coloring.

SUMMARY

The multiphase model results presented here, with accompanying animations, help to visualize the different flow and sedimentation phenomena and their impact on the formation of macrosegregation. Multiphase modeling provides a deeper insight in several relevant macrosegregation phenomena. The models discussed here may be considered preliminary and qualitative in nature as a result of the model assumptions and simplifications, thus some of the simulation results may not be suitable for quantitative comparisons with industry processes. Future work, however, will include the necessary refinements required to successfully create a multiphase model compatible with industrial castings.

ACKNOWLEDGEMENTS

References

1. M. C. Flemings, "Our Understanding of Macrosegregation: PAST and Present," *ISIJ Int.*, 40(9) (2000), pp.833-841.
2. C. Beckermann, "Modeling of macrosegregation: applications and future needs," *Inter. Mater. Rev.*, 47(5) (2002), pp. 243-261.
3. G. Lesoult, "Macrosegregation in steel strands and ingots: Characterization, formation and consequences," *Mater. Sci. Eng. A*, 413-414 (2005), pp. 19-29
4. I. Ohnaka, "Microsegregation and Macrosegregation," *Metals Handbook: Vol. 15 Casting*, (USA: ASM International, 1998), pp. 136-141.
5. M. Wu, A. Ludwig, M. Pelzer and U. Postl, "On the Impact of Macroscopic Phase Separation on Solidification and Microstructures," *Adv. Eng. Mater.*, 7(9) (2005), pp.846-851.

6. A. Ludwig and M. Wu, "Modeling of Globular Equiaxed Solidification with a Two-Phase Approach," *Metall. Mater. Trans. A*, 33A (2002), pp. 3673-3683.
7. M. Wu, A. Ludwig, A. Bührig-Polaczek, M. Fehlbier, P. R. Sahm, "Influence of convection and grain movement on globular equiaxed solidification," *Inter. J. Heat Mass Transfer*, 46 (2003), pp. 2819-2832.
8. M. Wu and A. Ludwig, "A Three-Phase Model for Mixed Columnar-Equiaxed Solidification," *Metall. Mater. Trans. A*, 37A (2006), pp. 1613-1631.
9. M. Wu, A. Ludwig, and L. Ratke, "Modelling the solidification of hypermonotectic alloys," *Moell. Simul. Mater. Sci. Eng.*, 11 (2003), pp. 755-769.
10. M. Wu, A. Ludwig L. Ratke, "Modeling of Marangoni Induced Droplet Motion and Convection during Solidification of Hypermonotectic Alloys," *Metall. Mater. Trans. A*, 34A (2003), pp.3009-3019.
11. R. Mehrabian, M. Keane and M. C. Flemings, "Interdendritic Fluid Flow and Macrosegregation; Influence of Gravity," *Metall. Trans.*, 1(1970), pp. 1209-1220.
12. M. Wu, A. Ludwig, J. Luo, "Numerical study of the thermal-solutal convection and grain sedimentation during globular equiaxed solidification," *Mater. Sci. Forum*, 475-479 (1-5) (2005), p.2725-2730.
13. J. D. Hunt, "Steady State Columnar and Equiaxed Growth of Dendrites and Eutectic," *Mater. Sci. Eng.*, 65(1984), pp. 75-83.
14. J. Campbell, "Castings," (Butterworth Heinemann Ltd, Oxford, 1991), pp.151-158.